THE JOURNAL OF PHYSICAL CHEMISTRY C

Article

pubs.acs.org/JPCC

Fe_3O_4@Carbon Microsphere Supported Ag−Au Bimetallic Nanocrystals with the Enhanced Catalytic Activity and Selectivity for the Reduction of Nitroaromatic Compounds

Qiao An, Meng Yu, Yuting Zhang, Wanfu Ma, Jia Guo,* and Changchun Wang

State Key Laboratory of Molecular Engineering of Polymers, Department of Macromolecular Science, and Laboratory of Advanced Materials, Fudan University, Shanghai 200433, P. R. China

Supporting Information

ABSTRACT: The heterostructure Ag−Au bimetallic nanocrystals supported on Fe_3O_4@carbon composite microspheres were synthesized by one facile and controllable approach, wherein the Ag nanocrystals attached on the Fe_3O_4@carbon microspheres were prepared first and served as reductant for the galvanic replacement reaction with the Au precursor ($HAuCl_4$). Upon varying the feeding amounts of the Au precursor, the bimetallic compositions on the Fe_3O_4@carbon microsphere could be readily tuned resulting in a series of composite microspheres with different Au-to-Ag molar ratios. Subsequently, we thus investigated the catalytic activity and selectivity of the magnetic composite catalysts from two sides. First, 4-nitrophenol (4-NP) was applied as a model molecule to study the effect of different Au-to-Ag molar ratios on catalytic capabilities of the resulting composite microspheres. It was found that upon the addition of $NaBH_4$ the catalytic capability was markedly enhanced when the Au content was increased. The maximum activity parameter value reached 1580 s^{-1} g^{-1}, which is far higher than those of known monometallic composites. Also, they could give the equally high yields for other nitroaromatic compounds with various substituents, irrespective of the linked electron-donating or electron-withdrawing groups. Second, the synergistic effects of the carbon substrate in the catalysis reaction were demonstrated. When compared with colloidal SiO_2, TiO_2, and poly(styrene-*co*-acrylic acid) substrates, the carbon support not only facilitated the enhancement of the catalytic performance of the noble metal nanocrystals but was also more suitable for the *in situ* preparation of Au−Ag bimetallic nanocrystals using the GRR. Besides, the particles' convenience in terms of their magnetic separability and outstanding reusability was validated through many successive reduction reaction cycles. In light of these unique characteristics, the Fe_3O_4@C@Ag−Au composite microspheres show promising and great potential for practical applications.

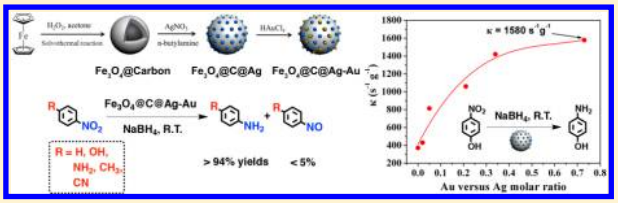

1. INTRODUCTION

Noble metal nanomaterials have attracted considerable attention due to their distinctive physicochemical properties and their potential for applications in the fields of biomedicine, catalysis, sensors, and electrochemistry.[1−7] In the past few decades, much effort has been dedicated to creating a diversity of methodologies for the controllable synthesis of noble monometallic nanocrystals with various shapes, including plates, rods, nanowires, and hollow spheres.[8−15] In contrast, little progress has been made in creating bimetallic nanostructures, likely because of the complicated and difficult approach required for the synthesis.[16−18] In comparison with the conventionally used solid and gaseous state routes (e.g., metallurgical techniques and molecular beam techniques), however, the solution-phase synthesis of bimetallic nanocrystals—including seeded growth, the galvanic replacement reaction, and noble-metal-induced reduction—is more feasible in operation and allows for the simple production of well-defined core/shell, heterostructure, or alloyed bimetallic nanocrystals by adjusting the reaction parameters. As such, the potential for an exciting range of applications now exists with this new family of bimetallic nanocrystals due to their exclusive electronic communication derived from the inherent nature of the two distinct metals.[19,20] In particular, for heterogeneous catalysis,[21] noble bimetallic nanocrystals (e.g., Pt−Au[22]) have been investigated as catalysts to confer an unprecedentedly improved catalytic capability, compared with monometallic nanocrystals. In a similar fashion, composite structures made of bimetallic nanocrystals and functionalized substrates have also attracted increasing attention. Bimetallic-nanocrystal-loaded composites are not only able to expose the active sites of the bimetallic nanocrystals but also to make use of the surface nature of the substrate to provide synergistic effects in the catalytic transformation of organic compounds. As far as we know, most methods use an *in situ* route, where the bimetallic nanocrystals are formed and concomitantly interact with the substrates. The obtained nanocrystals on substrates are usually mixtures composed of monometallic and bimetallic nanocrystals.[23−25] This may be a consequence of feeding the two metal precursors together, resulting in the uncontrollable growth of nanocrystals. Therefore, the locally controllable synthesis of bimetallic nanocrystals on the substrate is of vital

Received: August 1, 2012
Revised: September 27, 2012
Published: October 1, 2012

   dx.doi.org/10.1021/jp307629m | *J. Phys. Chem. C* 2012, 116, 22432−22440

Scheme 1. Fabrication Schematic Diagram of the Fe_3O_4@C@Ag−Au Composite Microspheres and the Reduced Protocol of 4-Nitrophenol by $NaBH_4$ Using Fe_3O_4@C@Ag−Au Composite Microspheres as Catalyst

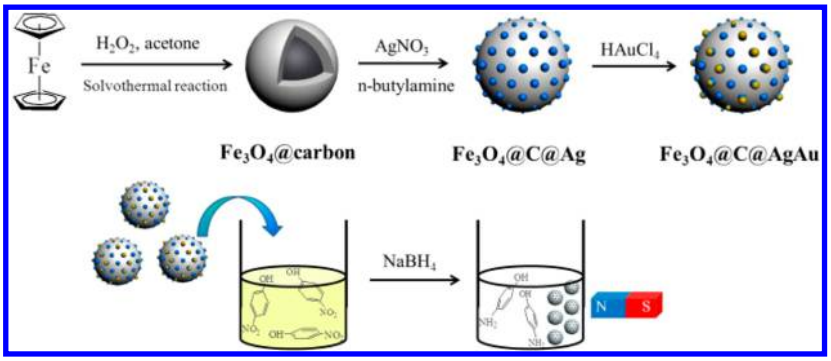

importance to allow the creation of bimetallic nanostructures within composites. Recently, porous materials (such as metal−organic frameworks, carbon spheres, etc.) have been utilized as high-surface-area supports for robustly anchoring the bimetallic nanocrystals within the micro- or mesoporous structures,[26−28] whereas their restriction effects lead to a limited catalytic activity of bimetallic nanocrystal-based solid catalysts. We thus propose that the catalytic capability of solid catalysts might be greatly enhanced if the bimetallic nanocrystals could densely cover the surface of supports. To this end, a dispersible and functionalized colloidal substrate may be suitable due to its tunable surface natures and particle sizes. However, there are very few studies conducted on exploration of the surface engineering of locally synthesized bimetallic nanocrystals by the galvanic replacement reaction (GRR).

Variable carbon nanomaterials with specific surface chemistries are one of the most widely used catalyst supports.[29,30] Studies have investigated the design of metallic composite structures using carbon nanotubes, graphene, and activated carbon.[31−33] High surface areas or appropriate pore sizes are offered by carbon substrates, and they are thus suitable for the accommodation of metal nanocrystals. Moreover, the nanoparticle distributions could be well modulated both inside and outside the carbon microspheres, allowing for control over their optical and catalytic properties.[27,28] At the meanwhile, it has been found that the carbon matrix has an effect in enhancing the catalytic activity and selectivity, as a result of the strong interaction between the substrate and the active phase. For example, bimetallic nanostructures supported on activated carbon showed higher activity and selectivity in the reduction of nitrate than an identical metallic phase supported on TiO_2, Al_2O_3, or ZrO_2.[34] Although the reaction mechanics are still unclear, it is likely that the unique surface chemistry of the carbon matrix is the main contributor. Therefore, it is imperative to examine whether the carbon-supported bimetallic nanocrystals are also applicable to the catalytic reduction of a broad range of nitroaromatic compounds by sodium borohydride,[35,36] not just the model molecules like 4-nitrophenol.

Fe_3O_4 nanoparticles with a rapid and sustainable magnetic response have been extensively investigated for a wide range of practical and potential applications[37−39] and recently gained much attention as supports for noble metal nanocrystals.[40−42] They are unique, in that their facile enrichment properties make it possible to selectively capture catalysts from an intricate heterogeneous system and ensure their recyclability. However, if Fe_3O_4 nanoparticles were directly used as support of noble metal, the magnetic carriers were intensively subjected to forced degradation in acidic condition or slow oxidation upon exposure to air. With this in mind, it was expected that the core/shell-structured composite carriers were designed by using Fe_3O_4 nanoclusters as core and functionalized carbon layer as shell, aiming at exploration of a more chemically and environmentally stable particle for supporting the bimetallic nanocrystals.

To accomplish the above, in this study we adopted the modified GRR for the *in situ* preparation of Ag−Au bimetallic nanocrystals on Fe_3O_4@carbon microspheres in solution. As shown in Scheme 1, ferrocene was used as a single iron source and was subjected to solvothermal treatment in the one-pot synthesis of Fe_3O_4@carbon microspheres. The obtained core/shell microspheres were applied to interact with Ag^+ ions, and in turn, *n*-butylamine was added for the reduction of local Ag^+ ions, resulting in the creation of Fe_3O_4@C@Ag microspheres. The fixed Ag nanocrystals on the surface of the Fe_3O_4@carbon microspheres served as a sacrificial template for the generation of Au via the GRR, which was finally responsible for the creation of the Ag−Au bimetallic heterostructures supported on the Fe_3O_4@carbon microspheres. By varying the feeding amounts of $HAuCl_4$, a fine control was obtained over the synthesis of the Ag−Au bimetallic nanocrystals supported on the Fe_3O_4@carbon composite microspheres. To investigate the catalytic capabilities of the bimetallic nanocrystals and the synergistic effects of the carbon substrate, we performed a detailed validation of the activity and selectivity of the Fe_3O_4@C@Ag−Au microspheres by applying them as a catalyst in the reduction of nitroaromatic compounds, with the assistance of sodium borohydride ($NaBH_4$). The advantages of the Fe_3O_4@C@Ag−Au microspheres in terms of their recoverability and reusability were demonstrated through many successive reduction reaction runs, under the application of an external magnetic field. Further insight into the synergistic effects of the sandwiched carbon layer in the catalysis reaction was explicitly obtained. Different colloidal substrates, including SiO_2, TiO_2, and poly(styrene-*co*-acrylic acid), were used to support equal loading of the bimetallic Ag−Au nanocrystals, using the same GRR-directed approach. Their catalytic behaviors were determined in the same reduction reaction, with aim of finding appropriate supports to optimize the catalytic performance of bimetallic nanocrystals.

2. EXPERIMENTAL SECTION

2.1. Reagents. Ferrocene ($Fe(C_5H_5)_2$, 99%), *n*-butylamine (99%), chloroauric acid (Au, 47.8%), nitrobenzene (99%), 4-nitrophenol (99%), 4-nitroaniline (99%), 4-nitrotoluene (99%),

dx.doi.org/10.1021/jp307629m | J. Phys. Chem. C 2012, 116, 22432−22440

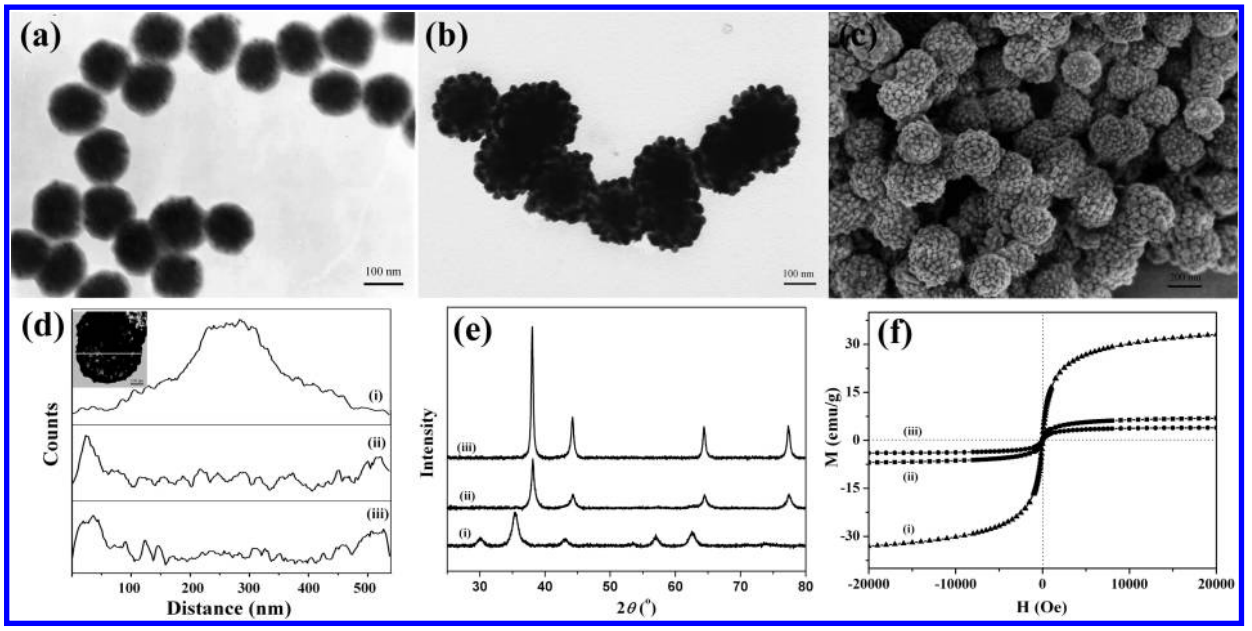

Figure 1. TEM images of Fe_3O_4@carbon microspheres (a) and Fe_3O_4@C@Ag microspheres (b); FE SEM image of Fe_3O_4@C@Ag−Au microspheres (c); EDX elemental line scanning profiles (d) corresponding to Fe (i), Ag (ii), and Au (iii), which are recorded along the line shown in the top inset of (d); PXRD patterns (e) of Fe_3O_4@carbon (i), Fe_3O_4@C@Ag (ii), and Fe_3O_4@C@Ag−Au (iii); magnetic hysteresis curves (f) of Fe_3O_4@carbon (i), Fe_3O_4@C@Ag (ii), and Fe_3O_4@C@Ag−Au (iii).

and 4-nitrobenzonitrile (≥97%) were purchased from the Aladdin Chemical Reagent Co., Ltd. Silver nitrate ($AgNO_3$, ≥99.8%) was obtained from the Shanghai Chemical Reagent Co., Ltd. Sodium borohydride ($NaBH_4$, 96%), hydrogen peroxide (H_2O_2, 30%), acetone (C_3H_6O, 99%), and anhydrous ethanol were purchased from the Sinopharm Chemical Reagent Co., Ltd. All chemicals were used as received without further purification. Highly pure water (Millipore) of resistivity greater than 18.0 MΩ·cm was used in all experiments.

2.2. Synthesis of Fe_3O_4@Carbon Microspheres. Fe_3O_4@carbon microspheres were prepared using the modified method as described previously.[43] In a typical procedure, 0.6 g of ferrocene was dissolved in 30 mL of acetone with vigorous sonication. 3.0 mL of H_2O_2 was slowly added into the above solution. The mixture was then magnetically stirred for 30 min. After that, the precursor solution was transferred to a 50 mL Teflon-lined stainless autoclave. The reaction was allowed to proceed for 24 h at 210 °C. The autoclave was then cooled to room temperature. The products were collected by a magnet and washed with acetone for three times to remove residual ferrocene. Finally, the purified products were redispersed in ethanol for further use.

2.3. Preparation of Fe_3O_4@C@Ag Microspheres. The *in situ* preparation of Ag nanocrystals was performed according to the method reported previously.[44] 5 mg of Fe_3O_4@carbon microspheres was dispersed using 15 mL of ethanol in a polypropylene container. 20 mM of $AgNO_3$ and 20 μL of *n*-butylamine were added into the solution, and the mixture was incubated for 50 min at 50 °C with vigorous shaking. The black products were rinsed with ethanol and dried in a vacuum oven.

2.4. Preparation of Fe_3O_4@C@Ag−Au Microspheres. Fe_3O_4@C@Ag−Au microspheres were prepared by the galvanic replacement method. Typically, 10 mg of Fe_3O_4@C@Ag microspheres was dispersed in 20 mL of ethanol, and the solution was transferred into a polypropylene container. A certain amount of $HAuCl_4$ (1 mM) was added, and the reaction was incubated at 50 °C for 1 h with vigorous shaking. The products were washed with the saturated NaCl solution and ethanol and dried in a vacuum oven.

2.5. Catalytic Reduction of 4-Nitrophenol (4-NP). The reduction of 4-NP was carried out in a quartz cuvette with an optical path length of 1 cm and monitored using UV−vis spectroscopy at 25 °C. 0.02 mL of aqueous 4-NP solution (5 mM) was mixed with 1.0 mL of a fresh $NaBH_4$ solution (0.02 M). 1.0 mL of aqueous dispersion of Fe_3O_4@C@Ag or Fe_3O_4@C@Ag−Au microspheres (0.001 wt %) was added, and the mixture solution was quickly measured by UV−vis spectroscopy. The change of absorption was recorded *in situ* to obtain the successive information about the reaction. As the reaction proceeded, it could be observed that the solution color changed gradually from yellow to colorless. In the recycling study, due to real-time measurement of UV absorption, the magnetic microspheres were magnetically separated out of the solution after the reduction reaction was completed. The obtained magnetic microspheres were washed with water and ethanol for three times and reused in the next reaction run. The procedure was repeated six times, and no significant decrease in product yields was found during the recycling test.

2.6. Catalytic Reduction of Nitroaromatic Compounds of Different Substituents. In a typical reaction, 0.6 mg of magnetic composite catalysts was added to 20 mL of aqueous solution containing 2.5 mM nitroaromatic compound and 250 mM $NaBH_4$. The mixture was stirred vigorously for 20 min at room temperature. After the magnetic microspheres were separated with a magnet, the product was extracted with diethyl ether and concentrated by a rotary evaporator for GC-MS analysis.

2.7. Catalysis Study by Using the Bimetallic Composite Catalysts with Different Substrates. The different substrates including poly(styrene-*co*-acrylic acid) (PSA), TiO_2, and SiO_2 were applied as the supporting materials for loading Ag−Au bimetallic nanocrystals. The synthesis of the PSA@Ag, TiO_2@Ag, and SiO_2@Ag microspheres was carried out according to the previous reports, and the supported Ag−Au

dx.doi.org/10.1021/jp307629m | J. Phys. Chem. C 2012, 116, 22432−22440

bimetallic nanocrystals were prepared by the same GRR strategy (see Supporting Information for details). The catalysis study of reduction of 4-NP with different catalysts was conducted in the same way as described above.

2.8. Characterization. Transmission electron microscopy (TEM) images were obtained on an H-600 (Hitachi, Japan) transmission electron microscope at an accelerating voltage of 75 kV. Scanning electron microscopy (SEM) images were recorded on a SUPERSCAN SSX-550 electron microscope (Shimadz, Japan) operating at 20 kV. A thin gold film was sprayed on the sample before measurements. Scanning transmission electron microscopy (STEM) images were obtained on a FE-SEM S-4800 (Hitachi, Japan) electron microscope at an accelerating voltage of 200 kV. The energy dispersive X-ray (EDX) spectroscopy was performed on the same transmission electron microscope with a QUANTAX 400 energy dispersive spectrometer (Bruker, Germany). Powder X-ray diffraction (PXRD) patterns were collected on a D8 advance (Bruker, Germany) diffraction meter with Cu KR radiation at λ = 0.154 nm operating at 40 kV and 40 mA. Magnetic characterization was carried out with a vibrating sample magnetometer on a Model 6000 physical property measurement system (Quantum Design) at 300 K. Ultraviolet−visible (UV−vis) absorption spectra were measured on a UV-3150 spectrometer (Shimadz, Japan). Since the metals in the sample could be dissolved by nitric acid completely, the metal contents were thus measured using inductively coupled plasma (ICP) spectrometry on a P-4010 ICP spectrometer (Hitachi, Japan). The reduction products and unconverted reactants were analyzed by a Focus DSQ gas chromatography−mass spectrometry (GC-MS; Thermoelectron) using HP-5MS capillary column and He as carrier gas. ζ-potential measurements were conducted with a Nano ZS Zetasizer (model ZEN3600, Malvern Instruments) using a He−Ne laser at a wavelength of 632.8 nm. The X-ray photoelectron spectroscopy (XPS) was performed using a PHI 5000C ESCA System X-ray photoelectron spectrometer.

3. RESULTS AND DISCUSSION

3.1. Synthesis and Characterization of Ag−Au Bimetallic Nanocrystals Supported on Fe_3O_4@Carbon Microspheres. The solvothermal synthesis of Fe_3O_4@carbon microspheres was performed using a one-pot method, following the modified method in a previous report.[43] As shown in Figure 1a, TEM images show well-defined core/shell composite microspheres, with a narrow size distribution and a mean diameter of ~160 nm. Close observation revealed that the gray carbon shell with a thickness of ca. 15 nm provided continuous coverage of the Fe_3O_4 nanoclusters. The resultant microspheres showed superior dispersibility in water, possibly owing to the presence of multiple functional groups on the surface of the carbon shell. We performed ζ-potential measurements and found that the negatively charged Fe_3O_4@carbon microspheres showed ζ-potentials of up to −33.0 mV. This indicated that the oxidation of carbon layers occurred under solvothermal conditions, and phenol or carboxylic acid groups were accordingly produced, leading to a relatively high surface charge and numerous coordinated sites for metal ions.[45] In comparison with polymer and silica shells, carbon shells exhibit much higher stability under harsh conditions, such as in acid or base medium, and at elevated temperatures or pressures. The magnetite core is protected from oxidation by the carbon shell, and the hydrophilic carboxyl groups are available for electrostatic interactions with the Ag^+ ions and consequently serve as nucleation sites for the deposition of Ag nanocrystals. *n*-Butylamine was used as a reducing agent to prepare Fe_3O_4@C@Ag microspheres. As is evident in Figure 1b, a large amount of nanoparticles with approximate sizes of 20−30 nm provided high coverage on the surface of the carbon shells. Then, the prepared Fe_3O_4@C@Ag microspheres were used as precursors to react with a $HAuCl_4$ solution, following the GRR, which has been demonstrated as a general and effective means for the synthesis of bimetallic nanostructures.[46] Since the standard reduction potential of the $AuCl_4^-$/Au pair (0.99 V vs standard hydrogen electrode, SHE) is higher than that of the Ag^+/Ag pair (0.80 V vs SHE), the loaded Ag nanocrystals were oxidized into Ag^+ with the addition of $HAuCl_4$ in aqueous solution, according to eq 1.

$$3Ag(s) + AuCl_4^-(aq) \rightarrow Au(s) + 3AgCl(s) + Cl^-(aq) \quad (1)$$

During this process, Au nanocrystals were produced and connected locally with the Ag nanoparticles on the surface of the Fe_3O_4@carbon microspheres; this happened gradually at the expense of the Ag nanocrystals. At the same time, Ag^+ ions were generated in the oxidation reaction, which simultaneously led to the precipitation of an AgCl solid. It has been reported that AgCl precipitate can be easily dissolved with a saturated NaCl solution through the coordination reaction (eq 2).[47]

$$AgCl(s) + 3Cl^-(aq) \rightarrow AgCl_4^{3-}(aq) \quad (2)$$

Figure 1c shows a representative SEM image of the Fe_3O_4@C@Ag−Au microspheres. It is evident that the surface of the Fe_3O_4@carbon microspheres was evenly covered with numerous nanoparticles, which apparently did not become unattached when the GRR was performed. To determine the composition of the synthesized bimetallic nanocrystals, EDX spectra were recorded, as shown in Figure S1 (see Supporting Information). The results revealed that the main peaks found in the spectrum were derived from Au, Ag, and Fe atoms, indicating that the composite microspheres contained the Au and Ag nanocrystals. Also, no signal for Cl was detected, implying that the AgCl solid byproduct was eliminated with the addition of the saturated NaCl solution. Additionally, the XPS spectrum in Figure S2 (see Supporting Information) shows the doublets $3d_{5/2}$ and $3d_{3/2}$ for Ag and $4f_{7/2}$ and $4f_{5/2}$ for Au, respectively, indicative of the bimetallic composition on the surface of composite microspheres again. More substantial evidence for the replacement of Ag with Au was given in the STEM-EDX line scanning measurement results. In Figure 1d, the element distribution profiles on the cross section behaved differently in elemental concentrations; Fe was abundant internally, and Au and Ag both appeared near the periphery of the microspheres. Again, this confirmed the structural characteristics of the resultant composite microspheres with a Fe_3O_4 core and an Ag−Au layer.

PXRD was applied to evaluate the crystalline property of the nanocrystals within the Fe_3O_4@C@Ag−Au microspheres. As displayed in Figure 1e, the synthesized Fe_3O_4@carbon microspheres gave X-ray diffraction peaks that could all be indexed to the cubic structure of Fe_3O_4 (JCPDS No.75-1609). As for the Fe_3O_4@C@Ag, the PXRD pattern showed four peaks at 38.18°, 44.39°, 64.58°, and 77.55°, which were indicative of characteristic diffractions due to the face-centered cubic structure of the Ag crystals (JCPDF No. 4-0783). A further examination of the Fe_3O_4@C@Ag−Au microspheres

dx.doi.org/10.1021/jp307629m | J. Phys. Chem. C 2012, 116, 22432−22440

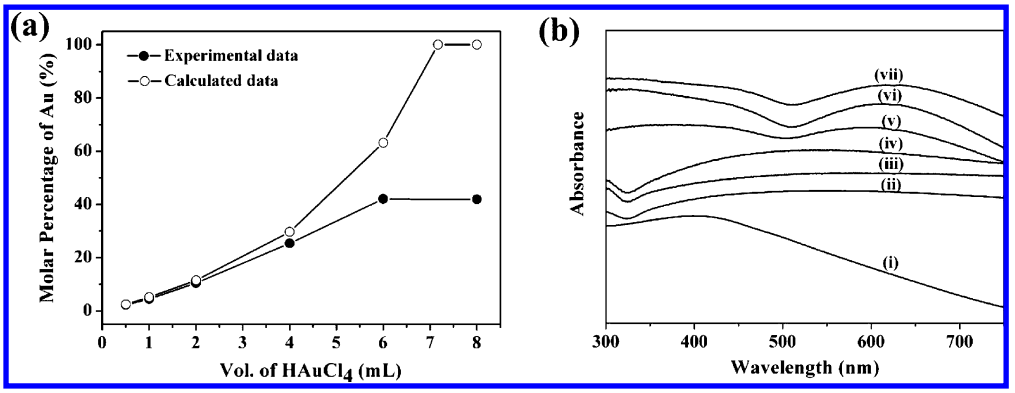

Figure 2. (a) Relationship between the molar percentage of Au in the Ag–Au bimetallic nanocrystals on Fe_3O_4@carbon and the volume of the $HAuCl_4$ solution (1 mM) summarized by experimental data and theoretical calculation. (b) The corresponding UV–vis absorption spectra of Fe_3O_4@carbon microspheres (i), Fe_3O_4@C@Ag microspheres (ii), and Fe_3O_4@C@Ag–Au microspheres synthesized by adding $HAuCl_4$ solution (1 mM) of 0.5 mL (iii), 1.0 mL (iv), 2.0 mL (v), 4.0 mL (vi), and 6.0 mL (vii).

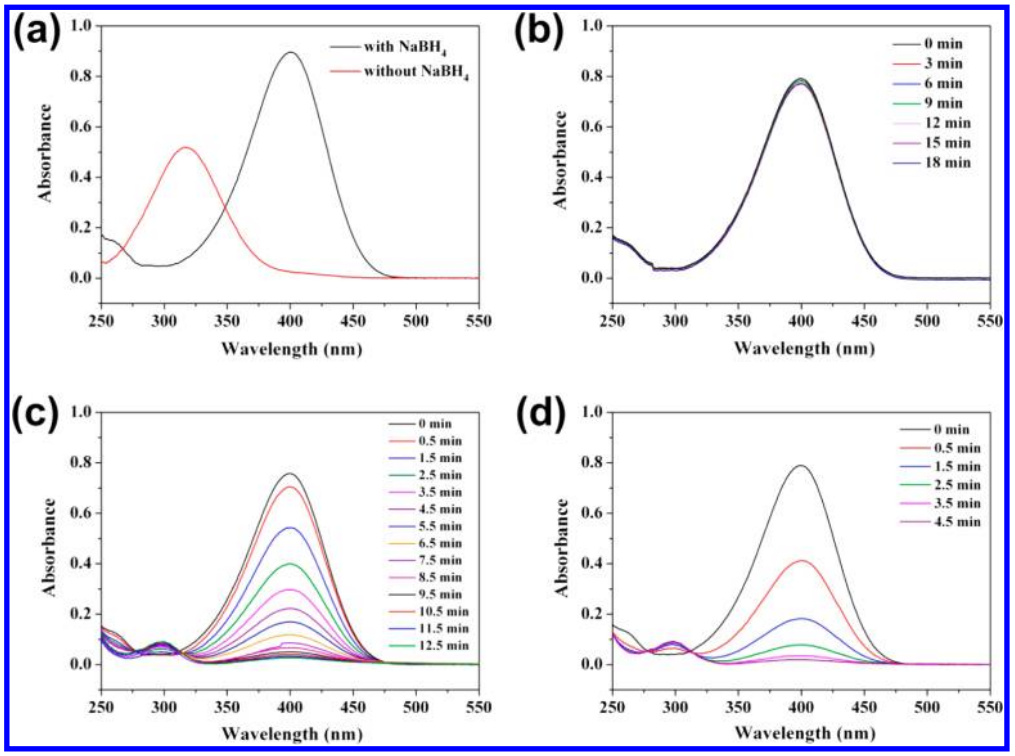

Figure 3. UV–vis spectra of 4-NP before and after addition of $NaBH_4$ solution (a), 4-NP with $NaBH_4$ without addition of any catalysts (b), 4-NP with $NaBH_4$ in the presence of Fe_3O_4@C@Ag microspheres as catalysts (c), and 4-NP with $NaBH_4$ in the presence of Fe_3O_4@C@Ag–Au microspheres as catalysts (d). The spectra of (b), (c), and (d) were all recorded in aqueous solution as the reduction of 4-NP proceeded.

showed that there was no obvious variation in peak positions, but there was a pronounced increase in intensity when the Ag–Au bimetallic nanocrystals were formed by the GRR. It was acceptable because the Ag and Au nanocrystals showed little difference in the PXRD pattern.[48]

The magnetization of the resulting microspheres was estimated using a vibrating sample magnetometer at 300 K. Figure 1f shows the magnetization hysteresis curves for the Fe_3O_4@carbon microspheres, the Fe_3O_4@C@Ag microspheres, and the Fe_3O_4@C@Ag–Au microspheres, respectively. The three similar curves revealed that the magnetization tended to decrease as a function of the applied magnetic field and approached saturated values as high as 33.4, 6.9, and 4.1 emu/g, respectively. Also, one can see that all of the curves nearly intersect with the origin; this feature showed that all of the samples were in a superparamagnetic state at room temperature.

To validate the synthetic controllability, ICP spectrometry was applied to quantitatively evaluate the percentages of Au and Ag within the Fe_3O_4@C@Ag–Au microspheres, by varying the feeding volume of $HAuCl_4$ solution (1 mM) under otherwise identical conditions. The curves in Figure 2a display the theoretically and experimentally determined changes in the Au concentrations. In comparison with the theoretical results calculated using the stoichiometric relationship in eq 1, the quantitative addition of $HAuCl_4$ solution could not oxidize the Ag nanocrystals into Ag^+ ions completely in the experiment. In the initial stage of the reaction, the Au contents increased as more of the $HAuCl_4$ solution was added. When the volume of the added $HAuCl_4$ solution was in excess of 6.0 mL, there was a

dx.doi.org/10.1021/jp307629m | J. Phys. Chem. C 2012, 116, 22432–22440

Table 1. Summary of the Activity Parameter κ Dependent on the Amounts of $HAuCl_4$ Solutions Added (1 mM), the Rate Constants of the Reaction (k), and the Au−Ag Weight and Molar Ratios

					Au/Ag		
sample	vol of $HAuCl_4$ (mL)	k (s^{-1})	Ag (wt %)	Au (wt %)	weight	molar	κ (s^{-1} g^{-1})
1	0.0	3.72×10^{-3}	23.20	0.00	0.00	0.00	372
2	0.5	4.31×10^{-3}	22.37	0.93	0.04	0.02	431
3	1.0	8.14×10^{-3}	20.34	1.71	0.08	0.05	814
4	2.0	10.61×10^{-3}	16.94	3.60	0.21	0.12	1061
5	4.0	14.22×10^{-3}	11.40	7.05	0.62	0.34	1422
6	6.0	15.80×10^{-3}	7.65	10.12	1.32	0.73	1580

maximum of 40 mol % of Au reduced by the deposited Ag on the microspheres, without further enhancement. This indicated that the redox reaction on the Fe_3O_4@carbon microspheres was incomplete, and a portion of the Ag nanocrystals remained with the newly synthesized Au nanocrystals. We reasoned that the simultaneous formation of AgCl solid could disrupt the epitaxial deposition of Au atoms on the surfaces of Ag seeds. Simultaneously, UV−vis spectra were used to monitor the replacement reaction between Ag and $HAuCl_4$, in light of the fact that the Au and Ag nanostructures exhibit the distinctive surface plasmon resonance peaks.[49] As shown in Figure 2b, when a small volume (0.5 and 1.0 mL) of $HAuCl_4$ solution (1 mM) was added to the dispersion of Fe_3O_4@C@Ag microspheres, the broad plasmon resonance peak red-shifted gradually. Subsequently, when the added amount of $HAuCl_4$ solution was increased to 2.0 mL, a new, well-resolved peak was observed at ∼610 nm. The absorption peak then red-shifted continuously to 630 nm as 4.0 and 6.0 mL of the $HAuCl_4$ solution were added. The change in the optical absorption spectra reflected the evolution of the chemical composition of the bimetallic nanocrystals supported on the Fe_3O_4@carbon microspheres.

3.2. Study of the Catalytic Reduction of Nitroaromatic Compounds Using Fe_3O_4@C@Ag−Au Microspheres. The reduction of 4-nitrophenol (4-NP) by $NaBH_4$ was chosen as a model reaction to study the catalytic performance of the multifunctional Fe_3O_4@C@Ag−Au microspheres. The reaction process was monitored by UV−vis spectrometry, as illustrated in Figure 3. The original aqueous 4-NP solution was light yellow in color and showed typical absorption at ∼317 nm. Upon the addition of $NaBH_4$, the absorption maximum shifted to 400 nm (Figure 3a) due to the formation of 4-nitrophenolate.[50] Nevertheless, there was no change in the intensity at 400 nm after 18 min (Figure 3b), indicating that it was difficult for the reduction to proceed without a catalyst. When 1.0 mg of the bimetallic composite microspheres was used, the reaction was completed in 30 s. It was so rapid that the process could not be monitored. We therefore reduced the amount of catalyst to 0.01 mg. Figure 3c shows the UV−vis spectra monitoring the reduction reaction of 4-NP, measured at different times using Fe_3O_4@C@Ag microspheres as the catalyst. The absorption peak at 400 nm gradually decreased in intensity as the reaction proceeded for 12.5 min; meanwhile, a new peak at 295 nm appeared and increased in intensity, which was ascribed to the typical absorption of 4-aminophenol (4-AP), the corresponding product in the reduction of 4-NP. Similarly, when 0.01 mg of the Fe_3O_4@C@Ag−Au microspheres (entry 3 in Table 1) was added, the absorption peak at 400 nm dramatically decreased in intensity after 4.5 min, and the peak at 295 nm increased accordingly (Figure 3d). In addition, the UV−vis spectra showed an isosbestic point (313 nm), suggesting that the catalytic reduction of 4-NP gave only 4-AP, without any other byproduct.[51]

Taking into account the much higher concentration of BH_4^- than 4-NP, the pseudo-first-order kinetics with respect to 4-NP can be applied to evaluate the catalytic activity of the Fe_3O_4@C@Ag−Au microspheres. The rate constant (k) was determined by a linear plot of $\ln(C_t/C_0)$ vs reduction time. The ratio of C_t to C_0, where C_t and C_0 are the 4-NP concentrations at time t and 0, respectively, was measured from the relative intensity of the respective absorbance, A_t/A_0. To gain insight into the effect of the Ag−Au bimetallic nanocrystals on the catalytic activity, we synthesized a series of microspheres with different ratios of Au to Ag, to compare the variation in their k values. As shown in Figure S3 (see Supporting Information), linear relations between $\ln(C_t/C_0)$ and the reduction time were observed for all samples, indicating that the reaction followed first-order kinetics. The rate constants, which were estimated from diffusion-coupled first-order reaction kinetics using the straight-line slopes, are summarized in Table 1. Although an increasing tendency could be observed in the k values as the Au contents increased, it is not entirely appropriate to compare different catalysts due to the direct effect of the used catalyst concentration on the rate constant. As such, the parameter $\kappa = k/m$—which is the ratio of the rate constant k to the total weight of catalyst added (0.01 mg)—was used to estimate the catalytic performance of the different catalysts. Table 1 presents the variable κ values, where the nature of the bimetallic nanocrystals in the composites was tuned by precisely controlling the Au/Ag molar ratios. Fe_3O_4@C@Ag microspheres were also tested as a control; they showed relatively poor catalytic performance, with the lowest activity index (κ = 372 s^{-1} g^{-1}). When the Ag−Au bimetallic nanocrystals were prepared on the Fe_3O_4@carbon microspheres, all the samples facilitated the improvement of the catalytic capability. With increases in the concentration of Au, κ accordingly increased, reaching values as high as 1580 s^{-1} g^{-1}. In contrast with prior reports, the catalytic activity κ of the Fe_3O_4@C@Ag−Au microspheres is the highest, as much as approximately 3−5 orders of magnitude higher than the values for Ag or Au monometallic composites.[52−54] We compiled the changing tendency of the κ values in Figure 4, with the aim of determining whether any correlation existed between the catalytic activity and the Au to Ag ratio. When the molar ratio of Au to Ag was varied from 0.02 to 0.73, the κ values first increased drastically and then eventually approached an asymptotic limit. It is most likely that the catalytic activity of the Ag−Au nanocrystals was enhanced with increased Au concentrations in the bimetallic nanocrystals, whereas a high coverage of the Ag template might have led to the transformation of the Ag−Au heterostructure into an Ag/Au core−shell structure. The stepwise changes of the bimetallic

dx.doi.org/10.1021/jp307629m | J. Phys. Chem. C 2012, 116, 22432−22440

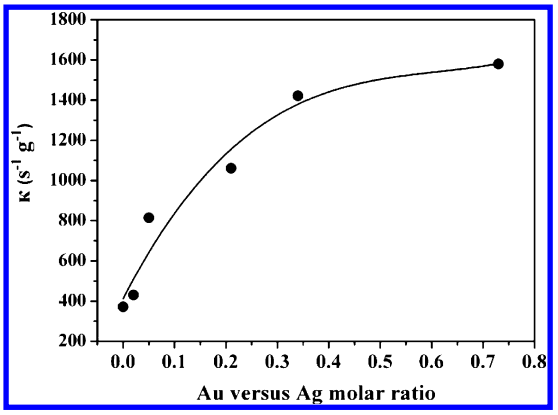

Figure 4. Relationship between the catalytic activity parameter (κ) and Au-to-Ag molar ratios when the noble metal nanocrystals supported on Fe_3O_4@carbon microspheres were transferred from Ag nanocrystals to Au–Ag bimetallic nanocrystals.

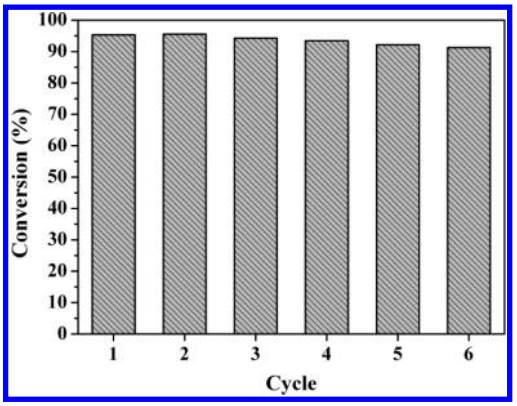

Figure 5. Reusability of the Fe_3O_4@C@Ag–Au microspheres (entry 6 in Table 1) as catalysts for the reduction of 4-NP by $NaBH_4$.

heterostructure could possibly account for the impairment of their catalytic efficacy.[25]

From the above analysis, it can be seen that the Fe_3O_4@C@Ag–Au microspheres showed outstanding catalytic activity, due largely to the nature of bimetallic nanocrystals supported on the Fe_3O_4@carbon microspheres. The Ag–Au heterostructure elicits an intimate contact between the Ag and Au and thus allows for an electronic communication that can activate the redox reaction.[55,56] Since the ionization potentials of Au and Ag are 9.22 and 7.58 eV, respectively,[57] electron transfer from Ag to Au would have occurred and may have resulted in a significant enhancement of the electron density on the surface of the catalytic microspheres. It was thus likely to activate the BH_4^- ions to capture the nitro group of the 4-NP molecule. The Ag–Au bimetallic nanocrystals immobilized on the surface of the Fe_3O_4@carbon microspheres were prepared without the addition of any ligands. Thus, the clean surface of the bimetallic nanocrystals could easily interact with the BH_4^- ions and 4-NP molecules, as a result of the exposure of catalytically active sites with electron-rich properties. All of these factors were conducive to the pronounced promotion of the catalytic capabilities of the catalysts.

To investigate the reusability and recoverability, the Fe_3O_4@C@Ag–Au microspheres with the highest catalytic activity (entry 6 in Table 1) were used in the reduction reaction of 4-NP, over six cycles. In this case, the Fe_3O_4 core enclosed within the microspheres was superbly useful in separating the catalysts out of the reaction mixture with the assistance of a magnet. As shown in Figure 5, high yields were attained in all six reaction runs, indicative of the recoverable catalytic activity of the Fe_3O_4@C@Ag–Au microspheres. We are aware of the slight decrease in conversion, which implies the possibility that the loaded Ag–Au bimetallic nanocrystals on the surface of the Fe_3O_4@carbon microspheres may leak off after many cycles in use.

Apart from 4-NP, we examined the scope and limitation of the reduction of nitro aromatic compounds, using the as-synthesized Fe_3O_4@C@Ag–Au microspheres as a catalyst. Nitro compounds can yield the nitroso form, which is regarded as a intermediate generated when a hydrogenation pathway to amine proceeds incompletely. All of the reactions indicated in Table 2 were completed very efficiently, giving excellent yields of the corresponding amine products. Regardless of the effects of electron-donating or electron-withdrawing functions, the high catalytic activities of the composite microspheres made all of the reactions proceed smoothly in a relatively short time. For comparison, the Fe_3O_4@C@Ag microspheres were used to catalytically reduce the same compounds. As displayed in Table S1 (see Supporting Information), compounds **1** and **4** were converted into an increased amount of the nitroso aromatic compounds. Moreover, it was found that 4-nitrobenzonitrile (compound **5**) could not be reduced using the Fe_3O_4@C@Ag microspheres, in sharp contrast to the broad catalytic selectivity of the bimetallic composite microspheres.

Table 2. Product Distributions (%) in the Reduction of Nitroaromatic Compounds Catalyzed by the Fe_3O_4@C@Ag–Au Microspheres (Entry 6 in Table 1)

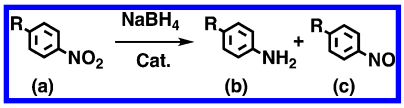

compd (R)	a	b	c[a]
1 (H)	<1	>99	
2 (OH)	<1	>99	
3 (NH_2)	<1	>99	
4 (CH_3)	<1	>94	5
5 (CN)	<3	>97	

[a]Uncertainties in these values are about 2%.

3.3. Comparison of Different Substrates for Ag–Au Bimetallic Nanocrystals in Terms of Catalytic Performance. To demonstrate the synergistic effect of the sandwiched carbon shell in the reduction reaction, common supporting materials—in the form of nanospheres made from poly(styrene-*co*-acrylic acid) (PSA), TiO_2, and SiO_2—were subjected to the same synthetic route used to prepare the PSA@Ag, TiO_2@Ag, and SiO_2@Ag microspheres, as a control. As shown in Figure S4 (see Supporting Information), the loaded Ag nanocrystals on the different substrates exhibited the various catalytic activities through the analysis of their rate constants attained from the changes of absorption. It was evident that the reduction of 4-NP catalyzed by the Fe_3O_4@C@Ag microspheres was rather faster than that observed with the other substrates. We assessed the weight percentage of Ag nanocrystals in microspheres using ICP. As listed in Table 3, the different substrates resulted in large differences in the content of loaded Ag nanocrystals. The coverage on the carbon was 2–3 times higher than that on the other substrates. Therefore, for a quantitative comparison, the activity parameter κ' was introduced, which is the ratio of the rate constant k to

dx.doi.org/10.1021/jp307629m | J. Phys. Chem. C 2012, 116, 22432–22440

Table 3. Effect of Different Substrates on the Activity Parameter κ' and the Loaded Amounts of Ag Nanocrystals and Ag−Au Bimetallic Nanocrystals

substrates	Ag (wt %)	κ' (s^{-1} g^{-1})[a]	substrates	Ag (wt %)	Au (wt %)	κ'' (s^{-1} g^{-1})[b]
Fe_3O_4@C@Ag	23.2	1603.4	Fe_3O_4@C@Ag−Au	7.65	10.12	8891.40
PSA@Ag	7.9	794.9	PSA@Ag−Au	2.14	3.84	18.90
TiO_2@Ag	9.5	405.1	TiO_2@Ag−Au	2.40	5.70	43.58
SiO_2@Ag	13.3	652.5	SiO_2@Ag−Au	0.80	1.23	8.37

[a]κ' is a ratio of rate constant (k) to weight of the loaded Ag nanocrystals. [b]κ'' is a ratio of rate constant (k) to weight of the loaded Ag−Au bimetallic nanocrystals.

the weight of Ag nanocrystals supported on the catalysts. Thus, when the added Ag content kept constant, the activity parameter κ' could be used to compare the effect of other factors on the catalytic activities, where the chemical nature of the substrates will be one of the main contributors. The results unambiguously showed that the carbon material did greatly facilitate the improvement of the catalytic activity, far better than the other substrates. Although the catalytic efficacy is influenced by many factors, we confirm that the carbon material is an adequate support for the *in situ* growth of Ag nanocrystals with high catalytic capability and that it might also show good selectivity in the reduction of nitroaromatic compounds, as a result of the specific interaction between nitrogen and aromaticity.

A further investigation involved the preparation of Ag−Au bimetallic nanocrystals supported on different colloidal substrates, using the reaction conditions applied in the synthesis of the Fe_3O_4@C@Ag−Au microspheres (entry 6 in Table 1). Figure S5 (see Supporting Information) shows the evolution of the absorption and the estimation of rate constants during the reduction of 4-NP using the SiO_2@Ag−Au, TiO_2@Ag−Au, and PSA@Ag−Au microspheres as catalysts, respectively. Analogically, the activity parameter κ'', a ratio of the rate constant k to the weight of Ag−Au bimetallic nanocrystals supported on the catalysts, was introduced. As presented in Table 3, the catalytic behaviors of the control catalysts were less pronounced or even completely absent. Also, the Ag and Au contents were notably different among those bimetallic composite microspheres. Although the GRR-directed synthesis of the Ag−Au bimetallic nanocrystals could be carried out on the PSA, TiO_2, and SiO_2 surfaces, the addition of the $HAuCl_4$ solution may have significantly affected the adhesion of the nanocrystals on the surface. A close look at the morphologies of the bimetallic composite microspheres (Figure S6) showed a remarkable conglutination or elimination of nanocrystals on the surface of microspheres, rather than the uniform distribution shown on the carbon matrix. This implied that the strong acidity of the Au precursor may have cleaved the coordinated bonds of the Ag nanocrystals with the hydroxyl groups of TiO_2 and SiO_2 or caused colloidal instability for PSA. The carbon substrate is more powerful as a support for bimetals in the galvanic replacement reaction; the numerous anchoring sites and antiacid structure can confine the formation of the bimetallic nanocrystals on the substrate well.

4. CONCLUSION

In conclusion, we synthesized a novel composite structure consisting of Fe_3O_4 nanoclusters as the core, functionalized carbon as a sandwich layer, and Ag−Au bimetallic nanocrystals as an outer shell. The Fe_3O_4@carbon microspheres acted as a support and were subjected to a facile and controllable method, the galvanic replacement reaction (GRR), for the synthesis of an Ag−Au heterostructure. Fe_3O_4@C@Ag composite microspheres were prepared and were reacted with $HAuCl_4$ to form Au on Ag nanocrystals. By varying the added amounts of the Au precursor, the Au-to-Ag molar ratios could be flexibly tuned using the GRR. Subsequently, the catalytic activity of the Fe_3O_4@C@Au−Ag microspheres was investigated in the reduction reactions of nitroaromatic compounds. A series of Fe_3O_4@C@Au−Ag microspheres with different Au-to-Ag molar ratios were applied as catalysts to reduce 4-nitrophenol, with the assistance of $NaBH_4$. Improved catalytic activity was found when the Au contents were increased; the activity parameter showed values as high as 1580 s^{-1} g^{-1}, which was far better than other known monometallic composites. The catalytic capability for reduction was evaluated for different nitroaromatic compounds to demonstrate that the Fe_3O_4@C@Au−Ag catalysts were available for a broad range of nitro substrates, regardless of the existence of electron-donating or electron-withdrawing substituents. In addition, the synergistic effects of the carbon substrate in the catalytic reaction were clearly demonstrated. Colloidal SiO_2, TiO_2, and poly(styrene-*co*-acrylic acid) were used as supports for bimetallic nanocrystals and were subjected to the same reduction reaction of 4-nitrophenol. The results demonstrated that the carbon substrate was the best, not only as a catalyst support exhibiting selectivity in the reduction of nitro compounds but also as a synthetic substrate favoring the formation of bimetallic nanocrystals under GRR conditions. In addition, the magnetic separability and reusability of the composite microspheres were demonstrated over many successive reaction runs. It is therefore anticipated that this kind of multifunctional bimetallic composite nanostructure will have great potential for future practical applications.

■ ASSOCIATED CONTENT

Ⓢ Supporting Information

EDX and XPS spectra of Fe_3O_4@C@Ag−Au microspheres; estimation of the rate constants of various catalysts; product distributions in the reduction of nitroaromatic compounds using the Fe_3O_4@C@Ag microspheres as catalysts; UV−vis spectra for the reduction of 4-NP using SiO_2-, TiO_2-, or PSA-supported Ag or Au−Ag nanocrystals as catalysts; TEM images of various composite microspheres. This material is available free of charge via the Internet at http://pubs.acs.org.

■ AUTHOR INFORMATION

Corresponding Author

*E-mail guojia@fudan.edu.cn; Tel +86-21-51630304; Fax +86-21-65640293.

Notes

The authors declare no competing financial interest.

■ ACKNOWLEDGMENTS

We acknowledge the supports by National Natural Science Foundation of China (Grant No. 21004012), Doctoral Fund of Ministry of Education of China (Grant No. 20100071120007), Scientific Research Foundation for the Returned Scholars of Ministry of Education of China, and Fundamental Research Funds for the Central Universities.

■ REFERENCES

(1) Huang, M. H.; Mao, S.; Feick, H.; Yan, H. Q.; Wu, Y. Y.; Kind, H.; Weber, E.; Russo, R.; Yang, P. D. *Science* **2001**, *292*, 1897.
(2) Holland, B. T.; Blanford, C. F.; Stein, A. *Science* **1998**, *24*, 538.
(3) Zhang, J. Z.; Schwartzberg, A. M.; Norman, T.; Grant, C. D.; Liu, J.; Bridges, F.; Buuren, T. V. *Nano Lett.* **2005**, *5*, 809.
(4) Wang, Z. L.; Song, J. H. *Science* **2006**, *312*, 242.
(5) Schwartzberg, A. M.; Zhang, J. Z. *J. Phys. Chem. C* **2008**, *112*, 10323.
(6) Li, J. H.; Zhang, J. Z. *Coord. Chem. Rev.* **2009**, *253*, 3015.
(7) Lu, L. H.; Wang, H. S.; Zhou, Y. H.; Xi, S. Q.; Zhang, H. J.; Hu, J. W.; Zhao, B. *Chem. Commun.* **2002**, 144.
(8) Xu, Z. H.; Hou, Y. L.; Sun, S. H. *J. Am. Chem. Soc.* **2007**, *129*, 8698.
(9) Nikoobakht, B.; El-Sayed, M. A. *Chem. Mater.* **2003**, *15*, 1957.
(10) Xia, Y. N.; Sun, Y. G. *J. Am. Chem. Soc.* **2004**, *126*, 3892.
(11) Kim, I.; Li, H.; Jo, J.; Wang, J.; Zhang, L. *Cryst. Growth Des.* **2010**, *10*, 5319.
(12) Xia, Y. N.; Zeng, J.; Zhang, Q.; Chen, J. Y. *Nano Lett.* **2010**, *10*, 30.
(13) Warren, S. C.; Disalvo, F. J.; Wiesner, U. *Nat. Mater.* **2007**, *6*, 156.
(14) Li, Y. S.; Su, H. M.; Wong, K. S.; Li, X. Y. *J. Phys. Chem. C* **2010**, *114*, 10463.
(15) Deng, Y. H.; Yang, W. L.; Wang, C. C.; Fu, S. K. *Adv. Mater.* **2003**, *15*, 1729.
(16) Banin, U. *Nat. Mater.* **2007**, *6*, 625.
(17) Wang, D. S.; Peng, Q.; Li, Y. D. *Nano Res.* **2010**, *3*, 574.
(18) Hao, R.; Xing, R.; Xu, Z.; Hou, Y.; Gao, S.; Sun, S. *Adv. Mater.* **2010**, *22*, 2729.
(19) Habas, S. E.; Lee, H.; Radmilovic, V.; Somorjai, G. A.; Yang, P. *Nat. Mater.* **2007**, *6*, 692.
(20) Xu, D.; Liu, Z. P.; Yang, H. Z.; Liu, Q. S.; Zhang, J.; Fang, J. Y.; Zou, S. Z.; Sun, K. *Angew. Chem., Int. Ed.* **2009**, *48*, 4217.
(21) Wang, D. S.; Li, Y. D. *Adv. Mater.* **2011**, *23*, 1044.
(22) Song, S. Y.; Liu, R. X.; Zhang, Y.; Feng, J.; Liu, D. P.; Xing, Y.; Zhao, F. Y.; Zhang, H. J. *Chem.—Eur. J.* **2010**, *16*, 6251.
(23) Chassagneux, F.; Bois, L.; Simon, J. P.; Desroches, C.; Brioude, A. *J. Mater. Chem.* **2011**, *21*, 11947.
(24) Hosseinkhani, B.; Søbjerg, L. S.; Rotaru, A. E.; Emtiazi, G.; Skrydstrup, T.; Meyer, R. L. *Biotechnol. Bioeng.* **2012**, *109*, 45.
(25) Kaiser, J.; Leppert, L.; Welz, H.; Polzer, F.; Wunder, S.; Wanderka, N.; Albrecht, M.; Lunkenbein, T.; Breu, J.; Kümmel, S.; Lu, Y.; Ballauff, M. *Phys. Chem. Chem. Phys.* **2012**, *14*, 6487.
(26) Jiang, H. L.; Akita, T.; Ishida, T.; Haruta, M.; Xu, Q. *J. Am. Chem. Soc.* **2011**, *133*, 1304.
(27) Tang, S. C.; Vongehr, S.; Zheng, Z.; Liu, H. J.; Meng, X. K. *J. Phys. Chem. C* **2010**, *114*, 18338.
(28) Tang, S. C.; Vongehr, S.; Meng, X. K. *J. Mater. Chem.* **2010**, *20*, 5436.
(29) Sun, Y. Q.; Li, C.; Bai, H.; Xu, Y. X.; Yao, Z. Y.; Shi, G. Q. *Chem. Commun.* **2010**, *46*, 4740.
(30) Bai, H.; Li, C.; Shi, G. Q. *Adv. Mater.* **2011**, *23*, 1089.
(31) Hong, W. J.; Bai, H.; Xu, Y. X.; Yao, Z. Y.; Gu, Z. Z.; Shi, G. Q. *J. Phys. Chem. C* **2010**, *114*, 1822.
(32) Li, X. Y.; Wang, X.; Song, S. Y.; Liu, D. P.; Zhang, H. J. *Chem.—Eur. J.* **2012**, *18*, 7601.
(33) Soares, O. S. G. P.; Órfão, J. J. M.; Pereira, M. F. R. *Catal. Lett.* **2010**, *139*, 97.
(34) Sakamoto, Y.; Kamiya, Y.; Okuhara, T. *J. Mol. Catal. A* **2006**, *250*, 80.
(35) Zeng, J.; Zhang, Q.; Chen, J.; Xia, Y. N. *Nano Lett.* **2010**, *10*, 30.
(36) Wu, H. X.; Wang, P.; He, H. L.; Jin, Y. D. *Nano Res* **2012**, *5*, 135.
(37) Medeiros, S. F.; Santos, A. M.; Fessi, H.; Elaissari, A. *Int. J. Pharm.* **2011**, *403*, 139.
(38) Mouaziz, H.; Veyret, R.; Theretz, A.; Ginot, F.; Elaissari, A. *J. Biomed. Nanotechnol.* **2009**, *5*, 172.
(39) Montagne, F.; Mondain-monval, O.; Pichot, C.; Elaissari, A. *J Polym. Sci., Part A: Polym. Chem.* **2006**, *44*, 2642.
(40) Yu, H.; Chen, M.; Rice, P. M.; Wang, S. X.; White, R. L.; Sun, S. H. *Nano Lett.* **2005**, *5*, 379.
(41) Lee, Y. M.; Garcia, M. A.; Huls, N. A. F.; Sun, S. H. *Angew. Chem., Int. Ed.* **2010**, *49*, 1271.
(42) Lin, F. H.; Doong, R. A. *J. Phys. Chem. C* **2011**, *115*, 6591.
(43) Wang, H.; Chen, Q. W.; Yu, Y. F.; Cheng, K.; Sun, Y. B. *J. Phys. Chem. C* **2011**, *115*, 11427.
(44) Kim, K.; Choi, J. Y.; Lee, H. B.; Shin, K. S. *ACS Appl. Mater. Interfaces* **2010**, *2*, 1872.
(45) Wang, H.; Sun, Y. B.; Chen, Q. W.; Yu, Y. F.; Cheng, K. *Dalton Trans.* **2010**, *39*, 9565.
(46) Poter, L. A.; Choi, H. C.; Ribbe, A. E.; Buriak, J. M. *Nano Lett.* **2002**, *2*, 1067.
(47) Lampre, I.; Pernot, P.; Mostafavi, M. *J. Phys. Chem. B* **2000**, *104*, 6233.
(48) Wang, Y.; Zheng, J. M.; Fan, K. N.; Dai, W. L. *Green Chem.* **2011**, *13*, 1644.
(49) Jackson, J. B.; Westcott, S. L.; Hirsch, L. R.; West, J. L.; Halas, N. J. *Appl. Phys. Lett.* **2003**, *82*, 257.
(50) Pradhan, N.; Pal, A.; Pal, T. *Langmuir* **2001**, *17*, 1800.
(51) Deng, Y. H.; Cai, Y.; Sun, Z. K.; Liu, J.; Liu, C.; Wei, J.; Li, W.; Liu, C.; Wang, Y.; Zhao, D. Y. *J. Am. Chem. Soc.* **2010**, *132*, 8466.
(52) Xie, L.; Chen, M.; Wu, L. M. *J. Polym. Sci., Part A: Polym. Chem.* **2009**, *47*, 4919.
(53) Zhang, Z. Y.; Shao, C. L.; Zou, P.; Zhang, P.; Zhang, M. Y.; Mu, J. B.; Guo, Z. C.; Li, X. H.; Wang, C. H.; Liu, Y. C. *Chem. Commun.* **2011**, *47*, 3906.
(54) Kuroda, K.; Ishida, T.; Haruta, M. *J. Mol. Catal. A: Chem.* **2009**, *298*, 7.
(55) Toshima, N.; Ito, R.; Matsushita, T.; Shiraishi, Y. *Catal. Today* **2007**, *122*, 239.
(56) Ferrando, R.; Jellinek, J.; Johnston, R. L. *Chem. Rev.* **2008**, *108*, 845.
(57) Tokonami, S.; Morita, N.; Takasaki, K.; Toshima, N. *J. Phys. Chem. C* **2010**, *114*, 10336.